11-12-03A11:1

AFRL-SR-AR-TR-03-

0470

REPORT DOCUMENTATION PAGE

1. AGENCY USE ONLY (Leave Blank)	2. REPORT DATE 6/17/02	3. REPORT TYPE AND DATES COVERED Final Technical 02-01-98 to 11/30/00

4. TITLE AND SUBTITLE
Aerodynamic Shape Optimization Using Control Theory

5. FUNDING NUMBERS
Grant No: F49620-98-1-0222

6. AUTHOR(S)

Professor Antony Jameson

7. PERFORMING ORGANIZATION NAME(S) AND ADDRESS(ES)

Stanford University
Aeronautics and Astronautics
Stanford, CA 94305-4030

8. PERFORMING ORGANIZATION REPORT NUMBER

9. SPONSORING / MONITORING AGENCY NAME(S) AND ADDRESS(ES)

Robert A.Canfield, LtCol
4015 Wilson Blvd., Rm 713
Arlington, VA 22203-1954

(WENDY VEN)
AIR FORCE OFFICE OF SCIENTIFIC RESEARCH

10. SPONSORING / MONITORING AGENCY REPORT NUMBER

Office of Naval Research
1107 N.E. 45h St., Suite 350
Seattle, WA 98105-4631

11. SUPPLEMENTARY NOTES
The views, opinions and/or findings contained in this report are those of the author(s) and should not be construed as an official Department of the Army position, policy or decision, unless so designated by other documentation.

12 a. DISTRIBUTION / AVAILABILITY STATEMENT
Approved for public release; distribution unlimited.

12 b. DISTRIBUTION CODE

13. ABSTRACT (Maximum 200 words)

The main objective of this work has been the development and maturation of a adjoint-based, viscous design techniques for Aerodynamic Shape Optimization (ASO) of complete aircraft configurations. We have followed a systematic approach in the development, validation and testing of our methods. In addition, we have carried out some preliminary work in the development of a mathematical environment for high-fidelity aero-structural optimization as a first step towards the realization of a high-fidelity multidisciplinary optimization capability. A number of significant milestones achieved in this process are detailed in the final report.

15. NUMBER OF PAGES
16

16. PRICE CODE

17. SECURITY CLASSIFICATION OR REPORT	18. SECURITY CLASSIFICATION ON THIS PAGE	19. SECURITY CLASSIFICATION OF ABSTRACT	20. LIMITATION OF ABSTRACT
UNCLASSIFIED	UNCLASSIFIED	UNCLASSIFIED	UL

NSN 7540-01-280-5500

Standard Form 298 (Rev.2-89)
Prescribed by ANSI Std. 239-18
298-102

Enclosure 1

20031121 014

ADVANCES IN AERODYNAMIC SHAPE OPTIMIZATION USING CONTROL THEORY

FINAL REPORT

AFOSR GRANT NO. AF F49620-98-1-0222

Antony Jameson and Juan J. Alonso
Department of Aeronautics & Astronautics
Stanford University
Stanford, CA 94305

1 Objectives

The main objective of this work has been the development and maturation of adjoint-based, viscous design techniques for Aerodynamic Shape Optimization (ASO) of complete aircraft configurations. We have followed a systematic approach in the development, validation and testing of our methods. In addition, we have carried out some preliminary work in the development of a mathematical environment for high-fidelity aero-structural optimization as a first step towards the realization of a high-fidelity multidisciplinary optimization capability. A number of significant milestones achieved in this process are detailed in this final report. Details of the work carried out can be found in a number of conference papers and archival publications that are quoted in the References section [1].

2 Summary

The effort to develop a framework for viscous aerodynamic shape optimization of complete aircraft configurations has yielded a number of important contributions during the length of this grant. The following sections reflect these contributions. We start with a thorough description of the adjoint equations for the compressible Reynolds-Averaged Navier-Stokes equations with some mention of implementation details. Once the first implementation of the viscous adjoint was completed, we carried out a thorough accuracy study of the gradients produced by the method with very encouraging results. In addition, we also spent much of the second year establishing the importance of continuous vs. discrete adjoint formulations. Our conclusions are detailed below and establish the validity of the continuous approach,

where we use the subscripts I and II to distinguish between the contributions associated with the variation of the flow solution δw and those associated with the metric variations δS. Thus $[\mathcal{M}_w]_I$ and $[\mathcal{P}_w]_I$ represent $\frac{\partial \mathcal{M}}{\partial w}$ and $\frac{\partial \mathcal{P}}{\partial w}$ with the metrics fixed, while $\delta\mathcal{M}_{II}$ and $\delta\mathcal{P}_{II}$ represent the contribution of the metric variations δS to $\delta\mathcal{M}$ and $\delta\mathcal{P}$.

In the steady state, the constraint equation specifies the variation of the state vector δw by

$$\delta R = \frac{\partial}{\partial \xi_i}\delta\left(F_i - F_{vi}\right) = 0. \tag{3}$$

Here, $R(w, S)$ is the residual of the flow equations, and F_i and F_{vi} are the inviscid and viscous fluxes. Here, also, δR, δF_i and δF_{vi} can be split into contributions associated with δw and δS using the notation

$$\delta R = \delta R_I + \delta R_{II} \tag{4}$$

$$\delta F_i = [F_{iw}]_I\,\delta w + \delta F_{iII}$$

$$\delta F_{vi} = [F_{viw}]_I\,\delta w + \delta F_{viII}. \tag{5}$$

Multiplying by a co-state vector ψ and integrating over the domain produces

$$\int_{\mathcal{D}} \psi^T \delta R d\mathcal{D}_\xi = \int_{\mathcal{D}} \psi^T \frac{\partial}{\partial \xi_i}\delta\left(F_i - F_{vi}\right) d\mathcal{D}_\xi = 0. \tag{6}$$

If ψ is differentiable the terms with subscript I may be integrated by parts to give

$$\int_{\mathcal{D}} \psi^T \delta R d\mathcal{D}_\xi + \int_{\mathcal{B}} n_i \psi^T \delta\left(F_i - F_{vi}\right)_I d\mathcal{B}_\xi \tag{7}$$

$$- \int_{\mathcal{D}} \frac{\partial \psi^T}{\partial \xi_i}\delta\left(F_i - F_{vi}\right)_I d\mathcal{D}_\xi = 0. \tag{8}$$

Since the left hand expression equals zero, it may be subtracted from the variation in the cost function (1) to give

$$\delta I = \delta I_{II} - \int_{\mathcal{D}} \psi^T \delta R_{II} - \int_{\mathcal{B}} \left[\delta\mathcal{M} - n_i \psi^T \delta\left(F_i - F_{vi}\right)_I\right] d\mathcal{B}_\xi$$

$$+ \int_{\mathcal{D}} \left[\delta\mathcal{P} + \frac{\partial \psi^T}{\partial \xi_i}\delta\left(F_i - F_{vi}\right)_I\right] d\mathcal{D}_\xi. \tag{9}$$

Now, since ψ is an arbitrary differentiable function, it may be chosen in such a way that δI no longer depends explicitly on the variation of the state vector δw. The gradient of the cost function can then be evaluated directly from the metric variations without having to recompute the variation δw resulting from the perturbation of each design variable.

Comparing equations (2) and (5), the variation δw may be eliminated from (9) by equating all field terms with subscript "I" to produce a differential adjoint system governing ψ

$$\frac{\partial \psi^T}{\partial \xi_i}\left[F_{jw} - F_{vjw}\right]_I + [\mathcal{P}_w]_I = 0 \quad \text{in } \mathcal{D}. \tag{10}$$

The corresponding adjoint boundary condition is produced by equating the subscript "I"

boundary terms in equation (9) to produce

$$n_x \psi^T \left[F_{j_w} - F_{v j_w} \right]_I = [\mathcal{M}_w]_I \quad \text{on } \mathcal{B}. \tag{11}$$

The remaining terms from equation (9) then yield a simplified expression for the variation of the cost function which defines the gradient

$$\delta I_{II} + \int_{\mathcal{D}} \psi^T \delta R_{II} d\mathcal{D}_\xi \tag{12}$$

The details of the formula for the gradient depend on the way in which the boundary shape is parameterized as a function of the design variables, and the way in which the mesh is deformed as the boundary is modified. Using the relationship between the mesh deformation and the surface modification, the field integral is reduced to a surface integral by integrating along the coordinate lines emanating from the surface. Thus the expression for δI is finally reduced to

$$\delta I = \int_{\mathcal{B}} G \, \delta S \, d\mathcal{B}_\xi = \mathcal{G} \delta \mathcal{F}, \tag{13}$$

where $\mathcal{F}$ represents the design variables, and $\mathcal{G}$ is the gradient, which is a function defined over the boundary surface. The advantage is that (13) is independent of δw, with the result that the gradient of I with respect to an arbitrary number of design variables can be determined with only a single flow-field evaluation and a single adjoint evaluation in a design cycle. Then, the computational cost of a single design cycle is roughly equivalent to the cost of two flow solutions since the adjoint problem has similar complexity. When the number of design variables becomes large, the computational efficiency of the control theory approach over the traditional approach (which requires direct evaluation of the gradients by individually varying each design variable and recomputing the flow field) becomes compelling.

Once equation (13) is established, an improvement can be made with a shape change

$$\delta \mathcal{F} = -\lambda \mathcal{G},$$

where λ is positive and small enough that the first variation is an accurate estimate of δI. Then

$$\delta I = -\lambda \mathcal{G}^T \mathcal{G} < 0.$$

After making such a modification, the gradient can be recalculated and the process repeated to follow a path of steepest descent until a minimum is reached.

The boundary conditions satisfied by the flow equations restrict the form of the left hand side of the adjoint boundary condition (11). Consequently, the boundary contribution to the cost function $\mathcal{M}$ cannot be specified arbitrarily. Instead, it must be chosen from the class of functions which allow cancellation of all terms containing δw in the boundary integral of equation (9). On the other hand, there is no such restriction on the specification of the field contribution to the cost function $\mathcal{P}$, since these terms may always be absorbed into the adjoint field equation (10) as source terms.

The detailed inviscid adjoint terms have been previously derived in [9, 10] and a detailed derivation of the viscous adjoint terms and the corresponding viscous adjoint boundary conditions can also be found in [2, 3, 11].

4 Accuracy and Cost Study of Viscous Adjoint-Based Gradients

A continuous adjoint method for Aerodynamic Shape Optimization (ASO) using the compressible Reynolds-Averaged Navier-Stokes (RANS) equations and the Baldwin-Lomax turbulence model was implemented and tested. The resulting implementation was used to determine the accuracy in the calculation of aerodynamic gradient information for use in ASO problems. The reader is referred to previous work [12] for details of the required mathematical derivations. The accuracy of the resulting derivative information is investigated by direct comparison with finite-difference gradients. The advantages of the use of an adjoint method over traditional finite-differencing become apparent because of the strict requirements that the finite difference method imposes on the level of flow solver convergence and the sensitivity of the value of the gradients with respect to the choice of step size. A parallel implementation using a domain decomposition approach and the MPI (Message Passing Interface) standard is used to reduce the computational cost of automatic design involving viscous flows.

As a result of this study, the following conclusions were reached:

- The flow solver convergence requirements for the finite difference method to produce accurate gradient information are quite severe and substantially increase the computational cost of this method.
- As opposed to what may be expected from direct truncation error analysis, the choice of step size for the calculation of derivatives using the finite difference method can cause a large error in the approximation of the gradients. Smaller step sizes (even disregarding the effect of roundoff error) are not necessarily better; the error in the resulting gradients depends on both the convergence level of the flow solver and the step size chosen.
- Gradient information obtained using the adjoint method is much less dependent on the level of convergence of the flow solver. Typically a convergence level 2 orders of magnitude larger than in the finite difference method can be tolerated.
- Gradient information obtained using the adjoint method is insensitive to the step size chosen in the deformation of the aerodynamic configuration.
- The adjoint method requires only modest levels of convergence (1.5 –2.5 orders) of the adjoint solver, thus reducing even further the computational cost of this procedure.
- Accurate gradient information can be obtained for flow governed by the RANS equations using the procedure outlined in previous work.

As a typical example of the results obtained during this study, Figure 1 shows the sensitivity of an inverse design cost function to the variations in 50 parameters that modify the shape of the airfoil. As can clearly be seen, the necessary level of convergence required for accurate gradients using a finite-difference approach is quite a bit higher than for the adjoint case. Not only is the cost of the adjoint procedure independent of the number of design variables

in the problem, but also , the cost of the flow solution is significantly reduced due to the less stringent convergence requirements.

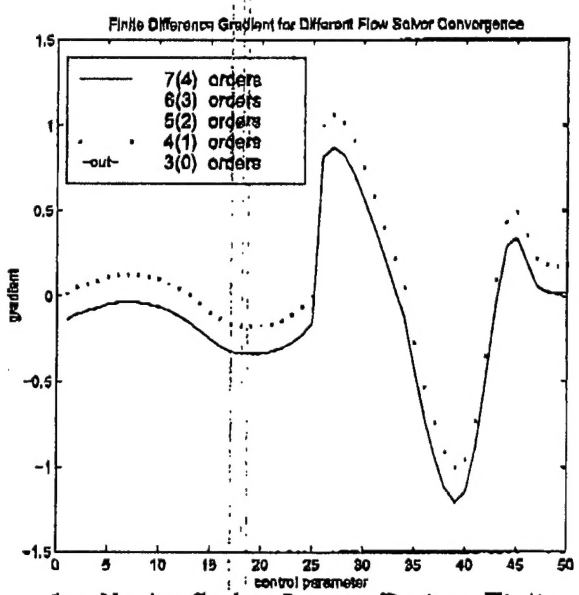

1a: Navier-Stokes Inverse Design: Finite Difference Gradients for Varying Flow Solver Convergence.

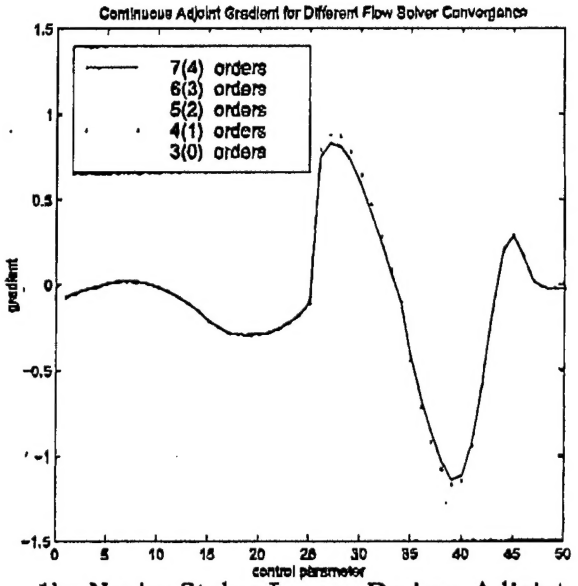

1b: Navier-Stokes Inverse Design: Adjoint Gradients for Varying Flow Solver Convergence.

5 Comparison of the Continuous and Discrete Adjoint Approaches to Automatic Aerodynamic Optimization

The objective of this study was to compare the continuous and discrete adjoint-based automatic aerodynamic optimization approaches. Our intention was to study the trade-offs between the complexity of the discretization of the adjoint equation for both the continuous and discrete approaches, the accuracy of the resulting estimates of the gradients, and their impact on the computational cost to approach an optimum solution. For details on the derivation and implementation of the continuous adjoint method, please refer to the cited bibliography. We will briefly present the complete formulation of the discrete adjoint equation and will then investigate their differences. The similarities between the continuous and discrete boundary conditions are also explored. The results demonstrate two-dimensional inverse pressure design as well as the accuracy of the sensitivity derivatives obtained from continuous and discrete adjoint-based equations when compared to finite-difference gradients. More details can be found in reference [13].

The discrete adjoint equation is obtained by applying the control theory directly to the set of discrete field equations. The resulting equation depends on the type of scheme used to solve the flow equations. The following discussion uses a cell centered multigrid scheme with upwind biased blended first and third order fluxes as the artificial dissipation scheme.

A full discretization of the equation would involve discretizing every term that is a function of the state vector

$$\delta I = \delta I_c + \sum_{i=2}^{n_x} \sum_{j=2}^{n_y} \psi_{i,j}^T \delta \left(R(w)_{i,j} + D(w)_{i,j} \right), \tag{14}$$

where δI_c is the discrete cost function, $R(w)$ is the field equation, and $D(w)$ is the artificial dissipation term.

Terms multiplied by the variation $\delta w_{i,j}$ of the discrete flow variables are collected and the following is the resulting discrete adjoint equation,

$$\begin{aligned}
&V \frac{\partial \psi_{i,j}}{\partial t} = \\
&\left(\Delta y_{\eta_{i+\frac{1}{2},j}} \left[\frac{\partial f}{\partial w} \right]_{i,j}^T - \Delta x_{\eta_{i+\frac{1}{2},j}} \left[\frac{\partial g}{\partial w} \right]_{i,j}^T \right) \frac{\psi_{i+1,j}}{2} \\
&- \left(\Delta y_{\eta_{i-\frac{1}{2},j}} \left[\frac{\partial f}{\partial w} \right]_{i,j}^T - \Delta x_{\eta_{i-\frac{1}{2},j}} \left[\frac{\partial g}{\partial w} \right]_{i,j}^T \right) \frac{\psi_{i-1,j}}{2} \\
&+ \left(\Delta x_{\xi_{i,j+\frac{1}{2}}} \left[\frac{\partial g}{\partial w} \right]_{i,j}^T - \Delta y_{\xi_{i,j+\frac{1}{2}}} \left[\frac{\partial f}{\partial w} \right]_{i,j}^T \right) \frac{\psi_{i,j+1}}{2} \\
&- \left(\Delta x_{\xi_{i,j-\frac{1}{2}}} \left[\frac{\partial g}{\partial w} \right]_{i,j}^T - \Delta y_{\xi_{i,j-\frac{1}{2}}} \left[\frac{\partial f}{\partial w} \right]_{i,j}^T \right) \frac{\psi_{i,j-1}}{2} \\
&- \left(\Delta y_{\eta_{i+\frac{1}{2},j}} \left[\frac{\partial f}{\partial w} \right]_{i,j}^T - \Delta x_{\eta_{i+\frac{1}{2},j}} \left[\frac{\partial g}{\partial w} \right]_{i,j}^T \right) \frac{\psi_{i,j}}{2} \\
&+ \left(\Delta y_{\eta_{i-\frac{1}{2},j}} \left[\frac{\partial f}{\partial w} \right]_{i,j}^T - \Delta x_{\eta_{i-\frac{1}{2},j}} \left[\frac{\partial g}{\partial w} \right]_{i,j}^T \right) \frac{\psi_{i,j}}{2} \\
&- \left(\Delta x_{\xi_{i,j+\frac{1}{2}}} \left[\frac{\partial g}{\partial w} \right]_{i,j}^T - \Delta y_{\xi_{i,j+\frac{1}{2}}} \left[\frac{\partial f}{\partial w} \right]_{i,j}^T \right) \frac{\psi_{i,j}}{2} \\
&+ \left(\Delta x_{\xi_{i,j-\frac{1}{2}}} \left[\frac{\partial g}{\partial w} \right]_{i,j}^T - \Delta y_{\xi_{i,j-\frac{1}{2}}} \left[\frac{\partial f}{\partial w} \right]_{i,j}^T \right) \frac{\psi_{i,j}}{2} \\
&+ \delta d_{i+\frac{1}{2},j} - \delta d_{i-\frac{1}{2},j} + \delta d_{i,j+\frac{1}{2}} - \delta d_{i,j-\frac{1}{2}},
\end{aligned} \tag{15}$$

where

$$\begin{aligned}
\delta d_{i+\frac{1}{2},j} &= \epsilon^2_{i+\frac{1}{2},j} (\psi_{i+1,j} - \psi_{i,j}) - \epsilon^4_{i+\frac{3}{2},j} \psi_{i+2,j} \\
&+ 3\epsilon^4_{i+\frac{1}{2},j} (\psi_{i+1,j} - \psi_{i,j}) + \epsilon^4_{i-\frac{3}{2},j} \psi_{i-1,j}
\end{aligned} \tag{16}$$

is the discrete adjoint artificial dissipation term and V is the cell area. The dissipation coefficients ϵ^2 and ϵ^4 are functions of the flow variables, but to reduce complexity they are treated as constants.

In the case of an inverse design, δI_c is the discrete form of the square of the pressure integral around the airfoil surface. In contrast to the continuous adjoint, where the boundary condition appears as an update to the costate variables in the cell below the wall, the discrete boundary condition appears as a source term in the adjoint fluxes. At cell $i, 2$ the adjoint

equation is as follows,

$$V\frac{\partial \psi_{i,2}}{\partial t} = \frac{1}{2}\left[-A^T_{i-\frac{1}{2},2}\left(\psi_{i,2}-\psi_{i-1,2}\right) - A^T_{i+\frac{1}{2},2}\left(\psi_{i+1,2}-\psi_{i,2}\right)\right] + \frac{1}{2}\left[-B^T_{i,\frac{5}{2}}\left(\psi_{i,3}-\psi_{i,2}\right)\right] + \Phi, \tag{17}$$

where V is the cell area, Φ is the source term for inverse design,

$$\Phi = \left(-\Delta y_\xi \psi_{2_{i,2}} + \Delta x_\xi \psi_{3_{i,2}} - (p-p_T)\Delta s_i\right)\delta p_{i,2},$$

and

$$A^T_{i+\frac{1}{2},2} = \Delta y_{\eta_{i+\frac{1}{2},2}}\left[\frac{\partial f}{\partial w}\right]^T_{i,2} - \Delta x_{\eta_{i+\frac{1}{2},2}}\left[\frac{\partial g}{\partial w}\right]^T_{i,2}.$$

All the terms in equation (17) except for the source term are scaled by the square of Δx. Therefore, as the mesh width is reduced, the terms within parenthesis in the source term divided by Δs_i must approach zero as the solution reaches a steady state. One then recovers the continuous adjoint boundary condition described in earlier works.

If a first order artificial dissipation equation is used, then equation (16) would reduce to the term associated with ϵ^2. In such a case, the discrete adjoint equations are completely independent of the costate variables in the cells below the wall. However, if we use the blended first and third order dissipation, then these values are required. In practice, a simple zeroth order extrapolation across the wall produces good results.

Replacing the inverse design boundary condition in equation (17) by the discrete form of the cost function results in a discrete adjoint equation for drag minimization.

As an example of the results in the study, an inverse design test case is briefly shown here. The target pressure is first obtained using the FLO83 flow solver for the NACA 64A410 airfoil at a flight condition of $M = 0.74$ and a lift coefficient of $C_l = 0.63$ on a 192 x 32 C-grid. At such a condition the NACA 64A410 produces a strong shock on the upper surface of the airfoil, thus making it an ideal test case for the adjoint versus finite difference comparison.

The gradient for the continuous and discrete adjoint is obtained by perturbing each point on the airfoil. We apply an implicit smoothing technique to the gradient, before it is used to obtain a direction of descent for each point on the surface of the airfoil.

Figures (1), (2), and (3) exhibit the values of the gradients obtained from the adjoint methods and finite difference for various grid sizes. The circles denote values that we obtain by using the finite difference method. The square represents the discrete adjoint gradient. The asterisk represents the continuous adjoint gradient. The gradient is obtained with respect to variations in Hicks-Henne sine "bump" functions placed along the upper and lower surface of the airfoil [14, 12]. The figures only illustrate the values obtained from the upper surface starting from the leading edge on the left and ending at the trailing edge on the right.

Figure (4) presents the effect of the partial discretization of the flow solver to obtain the discrete adjoint equation. Here we obtain the finite difference gradients in the figure

Grid Size	Cont.	Disc.	Cont-Disc
96 x 16	$3.106e-3$	$2.397e-3$	$9.585e-4$
192 x 32	$1.730e-3$	$1.724e-3$	$2.130e-4$
256 x 64	$1.424e-3$	$1.419e-3$	$4.749e-5$

Table 1: L_2 norm of the Difference Between Adjoint and Finite Difference Gradient

without freezing the dissipative coefficients. A small discrepancy exists in regions closer to the leading edge and around the shock.

Table 1 contains values of the L_2 norm of the difference between the adjoint and finite difference gradients. The table illustrates three important facts: the difference between the continuous adjoint and finite difference gradient is slightly greater than that between the discrete adjoint and finite difference gradient; the norm decreases as the mesh size is increased; and the difference between continuous and discrete adjoint gradients decreases as the mesh size is reduced. The second column depicts the difference between the continuous adjoint and finite difference gradient. The third column depicts the difference between the discrete adjoint and finite difference gradients. The last column depicts the difference between the discrete adjoint and continuous adjoint. As the mesh size increases the norms decrease as expected. Since we derive the discrete adjoint by taking a variation of the discrete flow equations, we expect it to be consistent with the finite difference gradients and thus to be closer than the continuous adjoint to the finite difference gradient. This is confirmed by numerical results, but the difference is very small. As the mesh size increases, the difference between the continuous and discrete gradients should decrease, and this is reflected in the last column of table 1.

In conclusion,

1. The continuous boundary condition appears as an update to the costate values below the wall for a cell-centered scheme, and the discrete boundary condition appears as a source term in the cell above the wall. As the mesh width is reduced, one recovers the continuous adjoint boundary condition from the discrete adjoint boundary condition.

2. Discrete adjoint gradients have better agreement than continuous adjoint gradients with finite difference gradients as expected, but the difference is generally small.

3. As the mesh size increases, both the continuous adjoint gradient and the discrete adjoint gradient approach the finite difference gradient.

4. The difference between the continuous and discrete gradient reduces as the mesh size increases.

5. The cost of deriving the discrete adjoint is greater.

6. With our search procedure as outlined, the overall convergence of the objective function is not significantly affected when the discrete adjoint gradient is used instead of the continuous adjoint gradient. Consequently, we find no particular benefit in using the discrete adjoint method, which requires greater computational cost. However, we

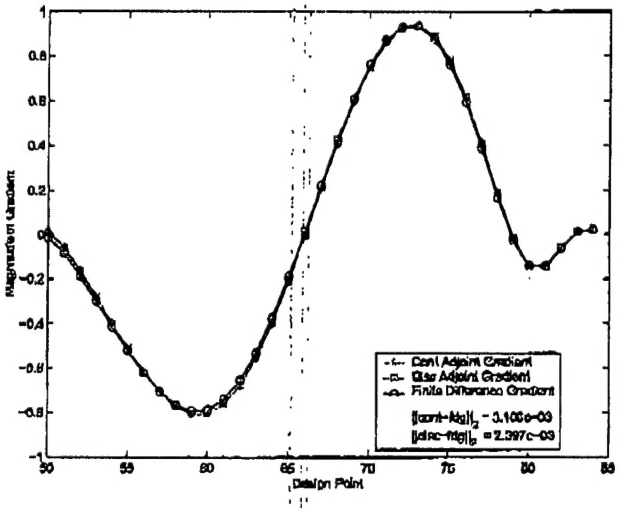

Figure 1: Adjoint Versus Finite Difference Gradients for Inverse Design of Korn to NACA 64A410 at Fixed C_l.

Coarse Grid - 96 x 16, $M = 0.74$, $C_l = 0.63$

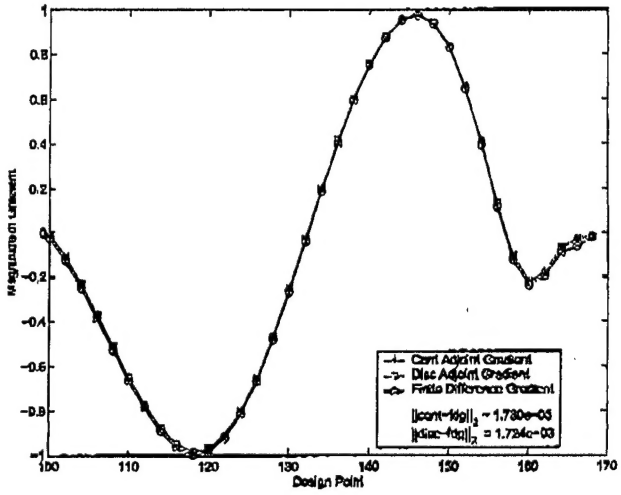

Figure 2: Adjoint Versus Finite Difference Gradients for Inverse Design of Korn to NACA 64A410 at Fixed C_l.

Medium Grid - 192 x 32, $M = 0.74$, $C_l = 0.63$

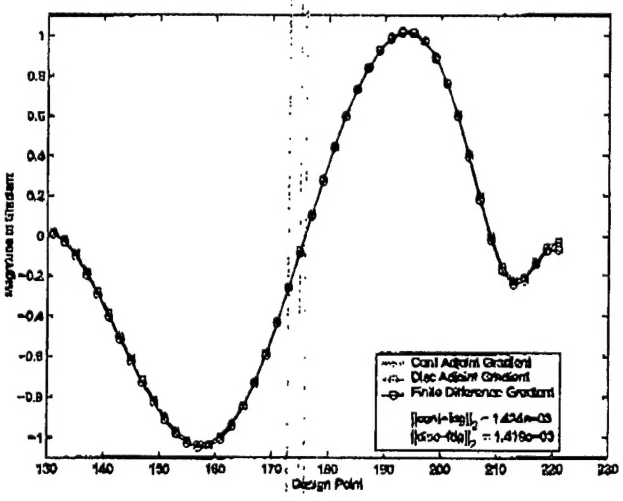

Figure 3: Adjoint Versus Finite Difference Gradients for Inverse Design of Korn to NACA 64A410 at Fixed C_l.

Fine Grid - 256 x 64, $M = 0.74$, $C_l = 0.63$

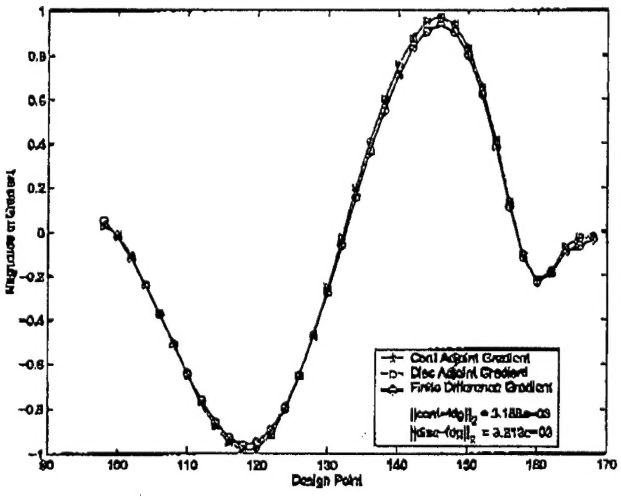

Figure 4: Adjoint Versus Finite Difference Gradients for Inverse Design of Korn to NACA 64A410 at Fixed C_l. Dissipative Coefficients Not Frozen

Medium Grid - 192 x 32, $M = 0.74$, $C_l = 0.63$

believe it beneficial to use the discrete adjoint equation as a guide for the discretization of the continuous adjoint equation.

6 Industrial Applications to Three-Dimensional Wing Design

During the period of this grant, the three-dimensional design method has been used successfully in some significant industrial applications at Boeing Long Beach. In addition to other similar efforts, the method was used to support the studies of the Blended-Wing-Body concept for long range transport aircraft which is under study at Boeing with Air Force and NASA support. The method was used to minimize the sum of the computed drag coefficients at Mach 0.85 at three lift coefficients in the range from 0.42 to 0.46. In order to check the results, Navier-Stokes calculations were performed using another CFD code, CFL3D, from NASA. These calculations verified an improvement in the lift to drag ratio over a range of lift coefficients from 0.35 to 0.68, with an improvement in the maximum lift to drag ratio of 4 percent. At the same time, the thickness of the outboard part of the wing was significantly increased, which could lead to benefits in reduced structural weight and increased fuel volume. The result of a similar calculation, checked with CFL3D, can be seen in the Figure below. The comparison is between the original design (dashed lines) and the optimized one (solid lines), resulting in more benign pressure distributions and an increase in lift-to-drag ratio of 4 %.

A second application was made to a high wing transport design under study at Long Beach. In this case the viscous wing design code was run for a single design point at Mach 0.85. A significant drag reduction was achieved with a calculation using 60 design cycles, with only 20 iterations of the flow solver and 20 for the adjoint solver in each design cycle. The total CPU time using 8 processors was 57613 seconds. A well converged analysis of the flow requires 400 iterations that amount to 7568 seconds with 8 SGI R10000 195 Mhz processors. Thus, the optimization was achieved at a cost of about 7.5 flow solutions. Again, a benefit in the lift to drag ratio was verified over a Mach number range form 0.845 to 0.865, with even greater benefit at the higher Mach number than at the design Mach number of 0.855. These results confirm the utility of the optimization method for real design applications. In industrial use, the ability to achieve optimizations with computational costs equivalent to 10 or even fewer flow solutions is crucial to the viability of the method. Research investigations which lead to the ability to construct design procedures with such low computational cost will be published in [15].

Other applications to supersonic configurations have also been presented, together with details of the algorithms, implementation, and parallelization [16, 17].

7 Preliminary Application to Aero-Structural Optimization

The work contained in the attached papers [16, 17, 18, 19] presents a new framework for the coupled optimization of aero-structural systems. The framework permits the use of high-

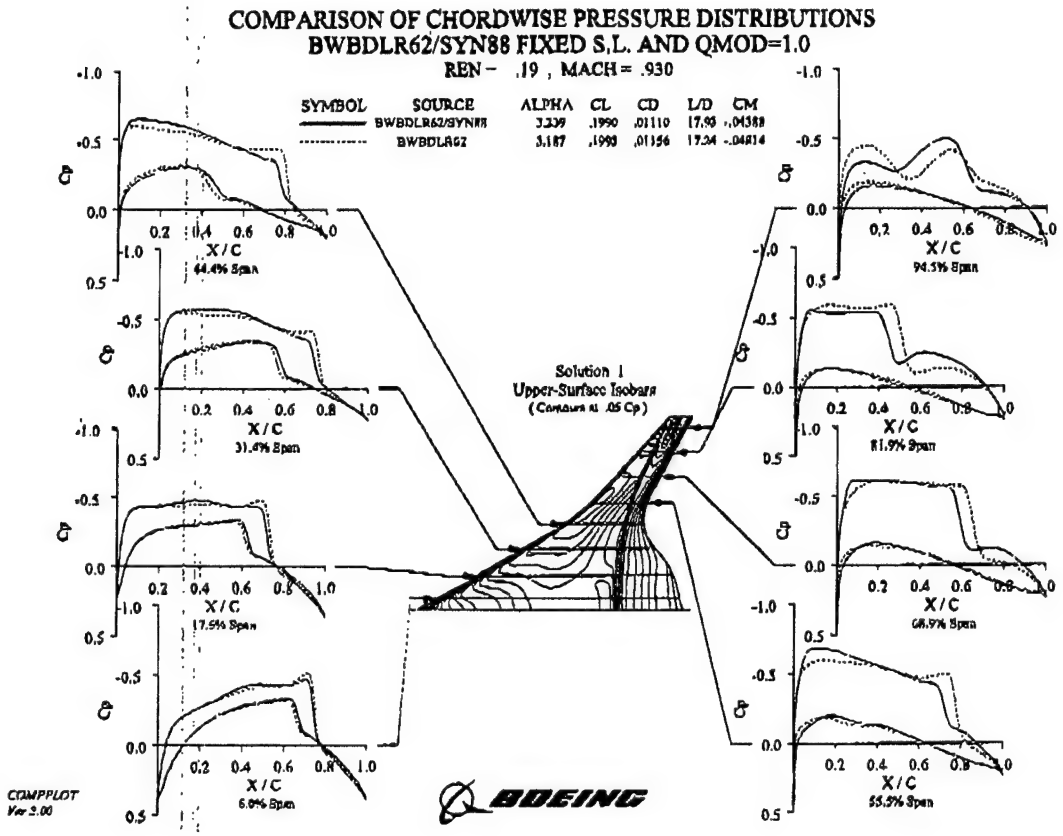

Figure 5: Sample Viscous Design for the Blended-Wing-Body Airplane.

fidelity modeling of both the aerodynamics and the structures and represents a first step in an effort towards the development of a high-fidelity multidisciplinary optimization capability. The approach is based on efficient analysis methodologies for the solution of the aerodynamics and structures subproblems, an adjoint solver to obtain aerodynamic sensitivities, and a multiprocessor parallel implementation. We have placed a geometry database representing the outer mold line (OML) of the configuration of interest at the core of our framework. Using this geometry description, the information exchange between aerodynamics and structures is accomplished through an independent coupling of each discipline with the OML database. The framework permits the later inclusion of other disciplines, such as heat transfer and radar signatures, with relative ease. Specific results from the coupling of a finite volume flow solver for the Euler and Reynolds Averaged Navier-Stokes equations with two different linear finite element structural models were explored. Care was taken in the treatment of the coupling of the disciplines such that a consistent and conservative scheme is achieved. Direct comparisons with wind-tunnel data were presented to demonstrate the importance of aeroelastic solutions. In addition, simplified design examples were presented to illustrate the possible advantages of the new aero-structural design methodology in evaluating trade-offs between aerodynamic performance and structural weight for complete aircraft configurations.

This design environment has been used to perform RANS aeroelastic analysis of complete configuration flight and wind-tunnel models with an additional cost which is less than 10% of the cost of a traditional rigid-geometry CFD solution. These solutions can be used to determine *a priori* whether significant aeroelastic corrections will or will not be needed for the resulting wind tunnel data.

In addition, simplified design cases have been tested that include the effect of aeroelastic deformations in the design process. These cases have shown that our design methodology is able to predict the correct trades between aerodynamic performance and structural properties present in these types of wing design problems.

Finally, a structural stress penalty function was added to the coefficient of drag of the complete configuration to allow elimination of artificial thickness constraints that are typically imposed in aerodynamic shape optimization methods. This rudimentary coupling of aerodynamics and structures in the design not only eliminates the necessity to impose artificial constraints, but also produces designs where trade-offs between aerodynamic and structural performance are considered.

Further work will focus on the continued development of the proposed MDO framework. Topics requiring significant research include sensitivity analysis, optimization strategy, Navier-Stokes based design, use of commercially available CSM codes, multipoint design, and CAD integration.

8 Personnel Supported

Funds from this grant have been used to support the time of Profs. Antony Jameson and Juan J. Alonso, and Mr. Siva Kumaran (Ph.D. Candidate in the department of Aeronautics & Astronautics).

9 Honors/Awards

Session Chairman. International Congress of Aeronautical Sciences (ICAS) 98 Congress, Sidney, Sept. 13-18, 1998. AJ

Invited Lecture. European Science Foundation Conference on Applied Mathematics for Industrial Flow Problems, San Feliu de Guixols, Spain, October 1-3, 1998. AJ

Invited Lecturer. Michigan State University Short Course on Computational Fluid Dynamics Modeling and Simulation, June 16-18, 1999. AJ

Lecturer. Fondazione CIME International Mathematical Summer Center, Course on "Computational Mathematics Driven by Industrial Applications", Martina Franca, Italy, June 21-27, 1999. AJ

Plenary Lecturer. 4th International Congress on Industrial and Applied Mathematics, ICIAM 99, Edinburgh, Scotland, July 5-9, 1999. AJ

Invited Lecture. Swedish Program in Scientific Computing Annual Meeting. Linkoping, Swe-

den. AJ

Invited Lecture. MIT Chautauqua Computational Fluid and Solid Mechanics. Cambridge, MA, June 2000. AJ

Member of NRC Committee on Naval Hydromechanics. Washington, DC. Report titled: "An Assessment of Naval Hydromechanics Science and Technology" issued. AJ

Session Chairman. International Congress of Aeronautical Sciences (ICAS) 2000 Congress, Harrogate, UK, August 2000. AJ & JJA

Session Chairman. AIAA Aerospace Sciences Meeting & Exhibit, Reno, NV, January 2000. JJA

Invited Lecture. Princeton University Mechanical & Aerospace Engineering Seminar Series, Princeton University, December 1999. JJA

Invited Panel Member. Computational Aerosciences Workshop, NASA Ames Research Center, April 2000. JJA

Invited Panel Member. High-Performance Scalability Workshop, Santa Fe, New Mexico. May 2000. JJA

Invited Panel Member. The History of CFD. AIAA Aerospace Sciences Meeting & Exhibit, Reno, NV, January 2000. AJ

Invited Panel Member. The Future of CFD. AIAA Fluids 2000 Conference, Denver, CO, June 2000. AJ

Invited Lecture. Computational Algorithms for Aerodynamic Analysis and Design. Fluent, Inc., Lebanon, NH, August 2000. AJ

Invited Lecture. Computational Algorithms for Aerodynamic Analysis and Design. EADS Munich, Germany, December 2000. AJ

Docteur Honoris Causa. University of Paris, December 2000. AJ

References

[1] A. Jameson and J. J. Alonso. Future research avenues in compuational engineering and design. In J. M. Ball and J. C. R. Hunt, editors, *Proceedings of the Fourth International Congress on Industrial and Applied Mathematics*, pages 79–95, Edinburgh, July 1999. Oxford University Press.

[2] A. Jameson, N. Pierce, and L. Martinelli. Optimum aerodynamic design using the Navier-Stokes equations. *AIAA paper 97-0101*, 35th Aerospace Sciences Meeting and Exhibit, Reno, Nevada, January 1997.

[3] A. Jameson, L. Martinelli, and N. A. Pierce. Optimum aerodynamic design using the Navier-Stokes equations. *Theoretical and Computational Fluid Dynamics*, 10:213–237, 1998.

[4] A. Jameson, J. J. Alonso, J. Reuther, L. Martinelli, and J. Vassberg. Aerodynamic shape optimization techniques based on control theory. *AIAA paper 2000-2598*, AIAA Fluid Dynamics Conference, Albuquerque, NM, June 2000.

[5] A. Jameson and L. Martinelli. Aerodynamic shape optimization techniques based on control theory. In *Lecture Notes in Mathematics, Vol. 1739*. Proceedings of Computational Mathematics Driven by Industrial Problems, Martina Franca, Italy, Springer-Verlag, 1999.

[6] A. Jameson, L. Martinelli, J. J. Alonso, J. C. Vassberg, and J. J. Reuther. Simulation based aerodynamic design. Technical report, IEEE Aerospace Conference, Big Sky, MT, March 2000.

[7] A. Jameson, J. J. Alonso, J. Reuther, L. Martinelli, and J. Vassberg. Computational fluid dynamics for the 21st century, perspectives on simulation based aerodynamic design. Computational fluid dynamics for the 21st century, Kyoto, Japan, July 2000.

[8] S. Kim, J. J. Alonso, and A. Jameson. Two-dimensional high-lift aerodynamic optimization using the continuous adjoint method. *AIAA paper 2000-4741*, 8th AIAA/USAF/NASA/ISSMO Symposium on Multidisciplinary Analysis and Optimization, Long Beach, CA, September 2000.

[9] A. Jameson and J. Reuther. Control theory based airfoil design using the Euler equations. *AIAA paper 94-4272*, 5th AIAA/USAF/NASA/ISSMO Symposium on Multidisciplinary Analysis and Optimization, Panama City Beach, FL, September 1994.

[10] A. Jameson. Aerodynamic design via control theory. *Journal of Scientific Computing*, 3:233–260, 1988.

[11] A. Jameson. A perspective on computational algorithms for aerodynamic shape analysis and design. In *Proceedings of the Sixth Taiwan National Conference on Computational Fluid Dynamics*, Taitung, Taiwan, ROC, August 1999. Elsvier.

[12] S. Kim, J. J. Alonso, and A. Jameson. A gradient accuracy study for the adjoint-based Navier-Stokes design method. *AIAA paper 99-0299*, 37th Aeospace Sciences Meeting and Exhibit, Reno, NV, January 1999.

[13] S. K. Nadarajah and A. Jameson. A comparison of the continuous and discrete adjoint approach to automatic aerodynamic optimization. *AIAA paper 2000-0667*, 38th Aerospace Sciences Meeting and Exhibit, Reno, Nevada, January 2000.

[14] R. M. Hicks and P. A. Henne. Wing design by numerical optimization. *Journal of Aircraft*, 15:407–412, 1978.

[15] A. Jameson and J. C. Vassberg. Studies of alternative numerical optimization methods applied to the brachistochrone problem. *OptiCON 99*, 1999.

[16] J. J. Reuther, A. Jameson, J. J. Alonso, M. Rimlinger, and D. Saunders. Constrained multipoint aerodynamic shape optimization using an adjoint formulation and parallel computers: Part I. *Journal of Aircraft*, 36(1):51–60, 1999.

[17] J. J. Reuther, A. Jameson, J. J. Alonso, M. Rimlinger, and D. Saunders. Constrained multipoint aerodynamic shape optimization using an adjoint formulation and parallel computers: Part II. *Journal of Aircraft*, 36(1):61–74, 1999.

[18] J. Reuther, J. J. Alonso, J. R. R. A. Martins, and S. C. Smith. A coupled aero-structural optimization method for complete aircraft configurations. *AIAA paper 99-0187*, 37th Aerospace Sciences Meeting and Exhibit, Reno, Nevada, January 1999.

[19] J. Reuther, J. J. Alonso, J. R. R. A. Martins, and S. C. Smith. A coupled aero-structural optimization method for complete aircraft configurations. Technical report, Canadian Aeronautics & Space Institute, Montreal, Canada, May 1999.